

UC Irvine

Faculty Publications

Title

Links between annual variations of Peruvian stratocumulus clouds and of SSTs in the eastern equatorial Pacific.

Permalink

<https://escholarship.org/uc/item/97r716pv>

Authors

Yu, J.-Y.
Mechoso, C. R.

Publication Date

1998-12-15

Copyright Information

This work is made available under the terms of a Creative Commons Attribution License, available at <https://creativecommons.org/licenses/by/4.0/>

Peer reviewed

Links between Annual Variations of Peruvian Stratocumulus Clouds and of SST in the Eastern Equatorial Pacific

JIN-YI YU AND CARLOS R. MECHOSO

Department of Atmospheric Sciences, University of California, Los Angeles, Los Angeles, California

(Manuscript received 14 July 1998, in final form 15 December 1998)

ABSTRACT

The hypothesis that Peruvian stratocumulus play an important role on both the annual mean and annual variations of sea surface temperature (SST) in the eastern equatorial Pacific is examined. The problem is addressed by performing sensitivity experiments using the University of California, Los Angeles, coupled atmosphere–ocean GCM with different idealized temporal variations of stratocumulus in a region along the coast of Peru.

The results obtained are consistent with the notion that Peruvian stratocumulus are a key component of the interhemispherically asymmetric features that characterize the annual mean climate of the eastern equatorial Pacific, including the cold SSTs off Peru and the absence of a southern ITCZ. The principal new finding of this study is that the annual variations (i.e., deviations from the annual mean) of Peruvian stratocumulus are linked to the differences between the amplitude, duration, and westward propagation of the warm and cold phases of the equatorial cold tongue. In the model's context, only if the prescribed annual variations of Peruvian stratocumulus have the same phase as the observed variations are those differences successfully captured.

The impact of Peruvian stratocumulus on equatorial SST involves “dynamical” and “thermal” effects. The former develop through an enhancement of the northerly component of the surface wind from the Peruvian coast to the equator. The thermal effects develop through the special relationships between SST and surface evaporation over the equatorial cold tongue, which contributes to extend the cold phase until the end of the year. A successful portrayal of this behavior requires a realistic simulation of the annual variations of surface wind over the equatorial cold tongue.

1. Introduction

The southern tropical Pacific and Atlantic Oceans are characterized by extensive and persistent low-level stratocumulus cloud decks off the coasts of South America and Africa. Recent studies have shown that those marine clouds can play important roles in the coupled atmosphere–ocean processes that characterize the climate of the Tropics. For example, Philander et al. (1996) pointed out that stratocumulus clouds off Peru contribute decisively to the meridional asymmetries in the climate of the tropical eastern Pacific, where sea surface temperatures (SSTs) are colder in the Southern Hemisphere than in the Northern Hemisphere. They suggested that feedbacks are at work by which SSTs are cooled down by those marine clouds, whose existence is in turn promoted by cooler SSTs. Ma et al. (1996) used a coupled atmosphere–ocean general circulation model (CGCM) to examine the sensitivity of the simulated climate to the amount of Peruvian stratocumulus. The approach in

that study was based on replacing the unrealistically low stratocumulus cloudiness produced by the model off Peru with constant overcast conditions. The enhanced stratocumulus resulted in a significant local cooling of the ocean surface due to shielding from solar radiation. In addition, the cooling extended northward to the south of the equator in the eastern tropical Pacific and westward along the equator in the central Pacific. Ma et al. (1996) found that the reasons for this remote cooling vary with location. The colder ocean surface underlying the stratocumulus resulted in increased zonal and meridional SST gradients and enhanced Walker and Hadley circulations. Consistently, there was increased surface evaporation and cooler SSTs immediately to the north of the region with artificially increased clouds. Oceanic advection propagated the cooling toward and along the equator.

The work of Ma et al. (1996) was performed in a highly idealized context. The constancy in time of the prescribed clouds, for example, precluded consideration of the potential effects of deviations from the annual mean (hereafter “annual variations”) in cloud cover. These variations exist in nature and are significant. Klein and Hartmann (1993) showed that the area coverage of low-level clouds off the coast of Peru varies from about

Corresponding author address: Dr. Jin-Yi Yu, Department of Atmospheric Sciences, University of California, Los Angeles, 405 Hilgard Ave., Los Angeles, CA 90095.
E-mail: yu@atmos.ucla.edu

40% in January–June to about 70% in July–December. The annual peak is in October when the atmospheric static stability is highest and local SSTs are lowest.

The present study extends the work of Ma et al. (1996) in a way that allows for an estimate of the effects of annual variations of Peruvian stratocumulus. Our approach is also based on sensitivity experiments with a CGCM. One of the experiments is a repeat of Ma et al. (1996), which is required in view of recent modifications in the model's code. In the others, Peruvian stratocumulus are enhanced either in the first or second-half of the calendar year. Hence, the annual variations of enhanced clouds in these two experiments are either out of phase or in phase with the observed, respectively. We focus particularly on how the annual variations of SST in the eastern equatorial Pacific are affected by different annual variations of Peruvian stratocumulus. In the former region, SST variations are characterized by a pronounced annual cycle. The seasonal cycle plays a key role in the coupled oscillations of the tropical atmosphere–ocean system that are at the root of the El Niño–Southern Oscillation (ENSO) phenomenon (Battisti and Hirst 1989; Neelin 1991). It also appears that the seasonal cycle plays an important role in determining the period, phase, and periodic nature of ENSO (Jin et al. 1994; Tziperman et al. 1994). This intimate dependency of anomalies on the mean state and seasonal cycle presents a major challenge to coupled GCM modelers.

The paper starts in section 2 by describing the CGCM, experiments performed, and observational data used for validation of results. Sections 3, 4, and 5 examine the impact of stratocumulus clouds on SST, wind stress, and surface heat fluxes at the equator, respectively. Section 6 discusses our results, and section 7 presents our conclusions.

2. Model, experiments, and data

a. Model description

The CGCM consists of the University of California, Los Angeles (UCLA), global atmospheric GCM (AGCM; Suarez et al. 1983; Mechoso et al. 1998; and references therein) and the Geophysical Fluid Dynamics Laboratory oceanic GCM (OGCM), which is the Modular Ocean Model (MOM; Bryan 1969; Cox 1984; Pacanowski et al. 1991). The AGCM includes the schemes of Deardorff (1972) for the calculation of surface wind stress and surface fluxes of sensible and latent heat, Katayama (1972) for shortwave radiation; Harshvardhan et al. (1987) for longwave radiation, Arakawa and Schubert (1974) for parameterization of cumulus convection, and Kim and Arakawa (1995) for parameterization of gravity wave drag. The model has a horizontal resolution of 4° lat \times 5° long and 15 layers in the vertical (with the top at 1 mb). The MOM includes the scheme of Mellor and Yamada (1982) for parameterization of

subgrid-scale vertical mixing by turbulence processes. The surface wind stress and heat flux are calculated hourly by the AGCM, and its daily averages passed to the OGCM. The SST is calculated hourly by the OGCM, and its value at the time of coupling is passed to the AGCM. The ocean model domain is from 30° S to 50° N and from 130° E to 70° W. There are 27 vertical layers and the depth is constant at 4150 m. The longitudinal resolution is 1° ; the latitudinal resolution varies gradually from $\frac{1}{2}^\circ$ between 10° S and 10° N to almost 3° at 30° S and 50° N.

In addition, the AGCM has larger values of emissivity for high-level clouds than those used in earlier studies (e.g., Robertson et al. 1995; Ma et al. 1996; Yu and Mechoso 1999). This modification reduces the excessive surface evaporation detected in previous model versions. When the AGCM is coupled to the OGCM, the modification slightly alleviates the cold SST bias in the extratropics that was obtained in earlier CGCM studies. The impact of increased emissivity for high-level clouds on equatorial SST will be discussed in the context of Fig. 2 of this paper. The reader is referred to Yu and Mechoso (1999) for an analysis of the relationships between heat flux errors in the AGCM and SST errors in the CGCM.

b. Simulations and sensitivity experiments

The four 5-yr-long CGCM integrations we perform consist of a control simulation (CTRL) and three hypothesis-testing experiments. CTRL produces unrealistically low amounts of stratocumulus everywhere, even at locations where SST is prescribed [see Ma et al. (1996) for a discussion on the model performance in simulating those clouds]. We first repeat the experiment designed by Ma et al. (1996), in which stratocumulus cloudiness is set to a constant 100% in all model grid points inside a domain between 10° and 30° S and from 90° W eastward to the Peruvian coast. The prescribed stratocumulus thickness is either 30 mb or that of the planetary boundary layer (PBL) if this is thinner than 30 mb. This repeat of Ma et al. (1996), which we will refer to as the “all-year experiment,” was performed in view of modifications made in the CGCM code since that paper was written. In the other experiments, the specification of 100% stratocumulus cloudiness is applied either from January through June (first-half-year experiment) or from July through December (second-half-year experiment).

The initial conditions for CTRL are taken from a CGCM simulation similar to that analyzed by Ma et al. (1996). The initial conditions for the all-year experiment correspond to 1 July of the second-year of CTRL. The initial conditions for the first-half-year and the second-half-year experiments both correspond to 1 July of the fourth year of the all-year experiment. The analyses presented in this paper were performed with the results obtained in the last three years of the integrations, in

which interannual variability was weak (see the appendix).

c. Observational data

The SST climatology used as the boundary condition for the AGCM outside the coupled domain is taken from Alexander and Mobley (1976). The surface heat flux, latent heat flux, and shortwave radiative flux used for validation are those compiled by Oberhuber (1988) from observational data mainly from the Comprehensive Ocean–Atmosphere Datasets (Woodruff et al. 1987) for the period 1950–79. The zonal and meridional components of the surface wind stress are those analyzed at The Florida State University (FSU; Legler and O'Brien 1984).

3. Impact on SST

Figure 1 shows the annual mean SST distribution from the observation as well as those obtained in CTRL and in the three experiments. CTRL simulates reasonable values of warm SST, although there is a warm bias, particularly in the eastern sector where SSTs can be up to 5°C warmer than observed along the coast of Peru. All three experiments obtain a more realistic SST distribution than CTRL. The strongest SST asymmetry about the equator is produced by the all-year experiment, in which the values between 0° and 10°S are about 4°C colder than in CTRL. The two half-year experiments obtain almost identical annual mean fields. They both have a weaker cooling of SSTs in the eastern sector south of the equator than the all-year experiment.

Figures 2a and 2b display profiles of SST zonally averaged between 120° and 90°W and meridionally averaged between 4°N and 4°S, respectively. According to Fig. 2a, CTRL simulates an almost symmetric SST distribution about the equator, with local maxima at about 6°N and 6°S. The all-year experiment reduces SSTs at all latitudes south of approximately 15°N. The reduction is particularly drastic south of the equator, which results in a strong interhemispheric asymmetry. These features are similar to those presented and discussed by Ma et al. (1996). The results obtained in the two half-year experiments are practically identical to each other. The cooling south of about 15°N is roughly one-half of that obtained in the all-year experiment. Note the similarity of results north of that latitude. Another aspect of interest is that all experiments produce a local SST maximum at about 6°S, where CTRL simulates a spurious intertropical convergence zone (ITCZ). Figure 2b shows again that CTRL produces too warm SSTs. Since this bias is stronger in the eastern sector, CTRL obtains the weakest SST gradients along the equator. This behavior differs drastically from that in the UCLA CGCM simulation reported by Mechoso et al. (1995). There, SSTs were consistently 2°–3°C too cold except just along the coast of South America, where

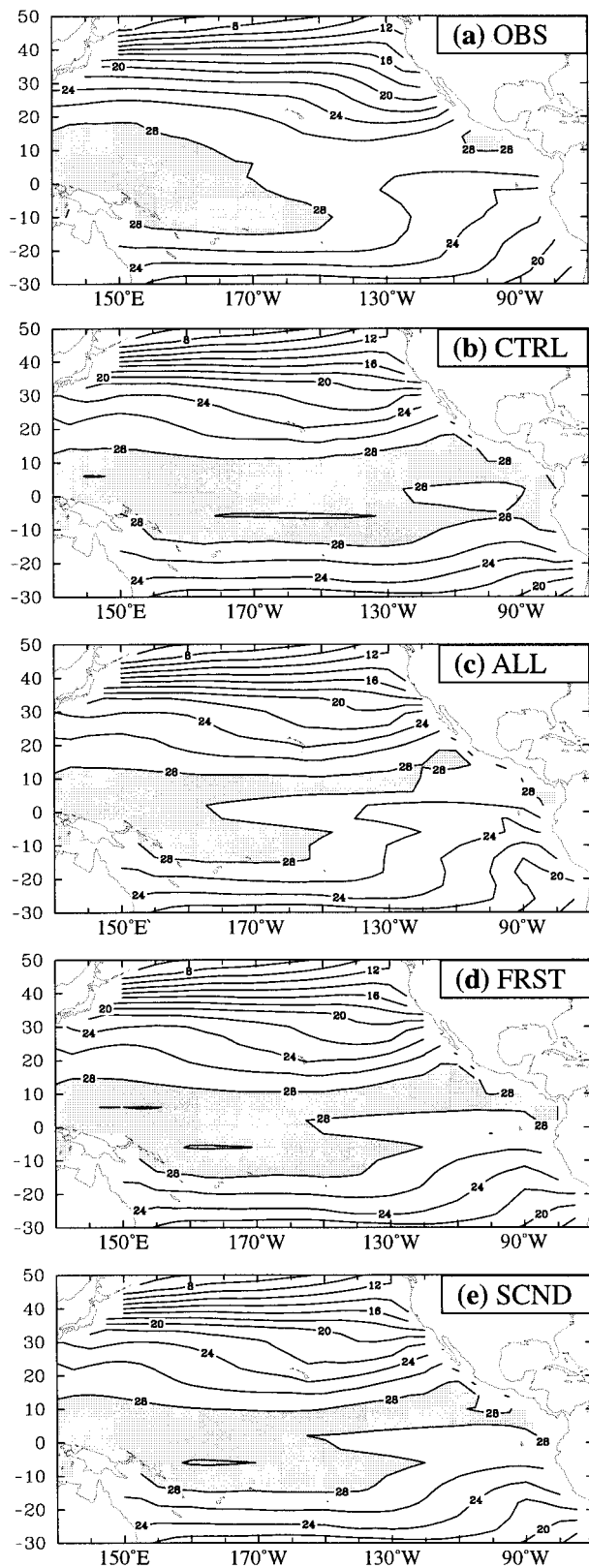


FIG. 1. Annual mean SST from (a) the observation and produced by the (b) control simulation (CTRL), (c) all-year experiment (ALL), (d) first-half-year experiment (FRST), and (e) second-half-year experiment (SCND). Contour interval is 2°C. Values larger than 28°C are shaded.

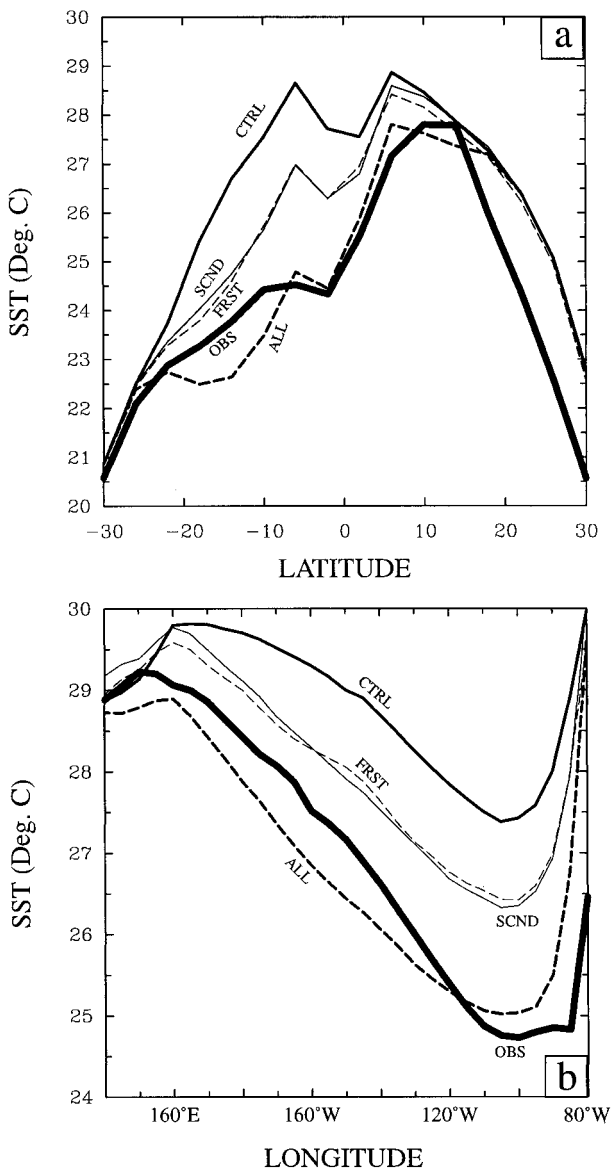


FIG. 2. Annual mean SST averaged (a) zonally between 120° and 90°W, and (b) meridionally between 4°N and 4°S, from the observation (thick solid line), the control simulation (medium solid line), the all-year experiment (medium dashed line), the first-half-year experiment (thin dashed line), and the second-half-year experiment (thin solid line).

they were too warm. Such a difference in behavior can be attributed to the larger emissivity for high-level clouds used in the later AGCM version. The new CTRL, therefore, is more appropriate for this investigation since the enhancement of stratocumulus should result in colder and more realistic SSTs, which is a step in the right direction. According to Fig. 2b, all the experiments produce colder SSTs in the central and eastern sectors. Again, the two half-year experiments obtain almost identical results. The most realistic distribution of an-

nual mean SST along the equator is produced by the all-year experiment.

Figures 1 and 2, therefore, suggest that Peruvian stratocumulus are associated with the cold annual mean SST in the eastern Pacific south of the equator. In view of the similarity between results obtained in the two half-year experiments, this cooling appears to depend more on the length than on the timing of the period in which those clouds are enhanced.

Figure 3 displays the annual variations of monthly mean SST at each longitude along the equator. In the observation (Fig. 3a), the variations are dominated by the semiannual harmonic in the western sector and by the annual harmonic in the eastern sector. Here, SSTs are larger than the annual mean from January through June and smaller from July through December. These warm and cold phases of the equatorial cold tongue differ from each other in strength, duration, and propagation characteristics. The warm phase is stronger and exhibits a clear westward propagation, but the cold phase lasts slightly longer and appears more stationary. We will refer to these differences as “temporal asymmetries.” Figures 3b–e show that all model integrations succeed in reproducing the dominance of the annual harmonic in the eastern sector. In CTRL (Fig. 3b), however, the warm phase of the equatorial cold tongue is too weak, while the cold phase is too strong and has a similar westward propagation. In addition, the cold phase ends earlier than in the observation. CTRL, therefore, simulates a much more symmetric behavior than the observation. The all-year experiment produces similar results albeit with weaker magnitudes. In the first-half-year experiment the cold phase is much stronger than the warm phase and has a clear westward propagation. It appears that only the second-half-year experiment produces differences between the strength, duration, and westward propagation of the warm and cold phases that broadly correspond to the observation.

To further examine the temporal asymmetries in the model’s equatorial cold tongue, we show in Fig. 4 the annual variations of SST averaged over 120°–90°W. The first-half-year experiment (Fig. 4c) has the most unrealistic annual variations over the cold tongue. The onset and termination, as well as the magnitude and duration, of the simulated warm and cold phases are very different from the observation. The annual variations produced by the second-half-year experiment (Fig. 4d) are the closest to the observation. In particular, the large peak value of the warm phase and the long duration of the cold phase are very well simulated. The all-year experiment also partially succeeds in alleviating the early termination problem of the cold phase seen in CTRL, but not as much as the second-half-year experiment. Table 1 lists the amplitude and phase of the annual harmonics in the distributions shown in Fig. 4. The amplitudes obtained in the second-half-year and first-half-year experiments are closer to the observation than the other simulations. However, the first-half-year experi-

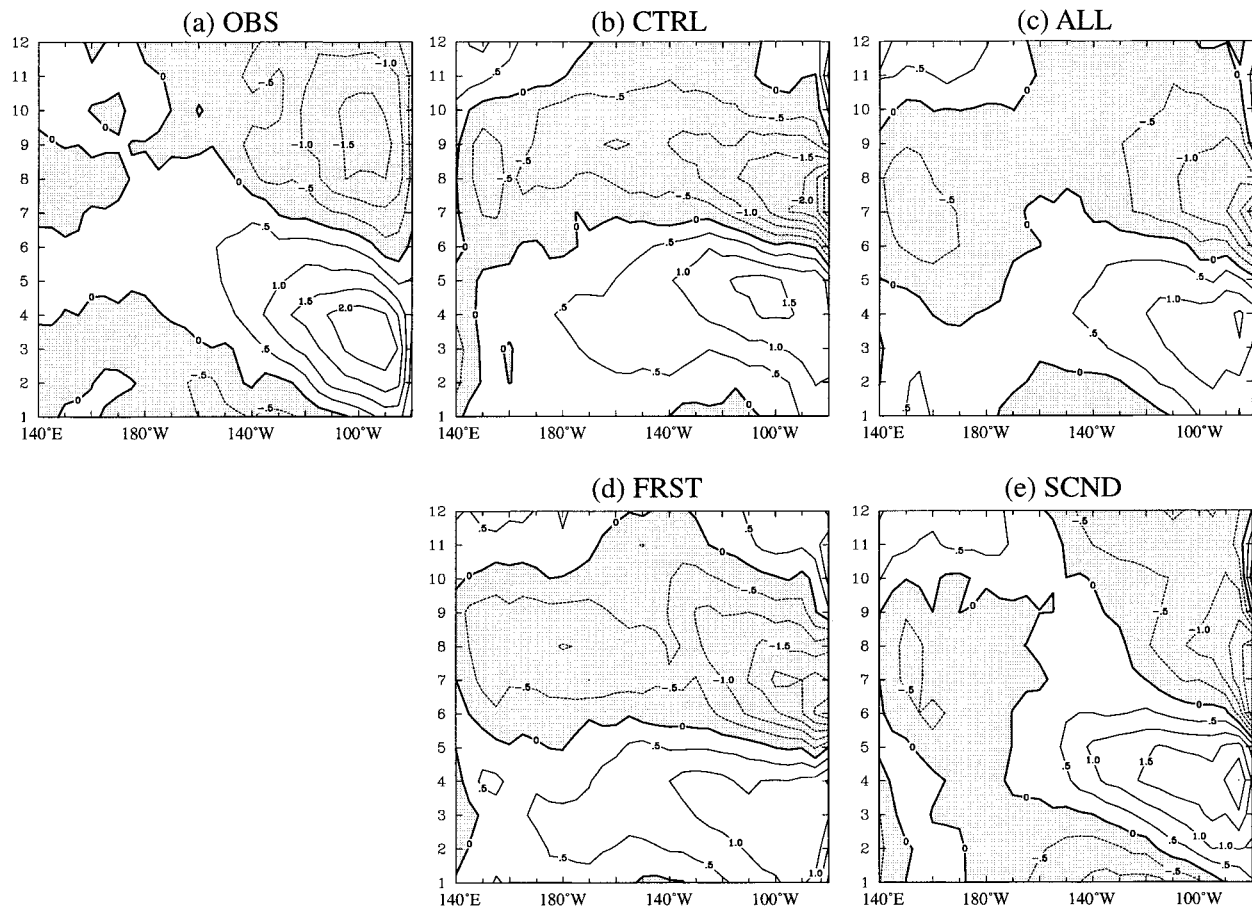


FIG. 3. Annual variations along the equator of monthly mean SSTs averaged between 4°S and 4°N from (a) the observation, (b) the control simulation, (c) the all-year experiment, (d) the first-half-year experiment, and (e) the second-half-year experiment. Contour interval is 0.5°C . Negative values are shaded.

ment produces an unrealistic phase for the annual harmonic. The phase obtained by the second-half-year experiment is similar to the observation. It is also noticed that the all-year experiment produces the weakest amplitude.

In summary, Figs. 3 and 4 show that the second-half-year experiment obtains the most realistic simulation of the amplitude, duration, and westward propagation features of both the warm and cold phases of the equatorial cold tongue. According to these results, there are links between the temporal asymmetries in the annual variations of SST over the eastern equatorial Pacific and in the annual variations of Peruvian stratocumulus.

4. Impact on surface wind stress at the equator

Figure 5 shows that the meridional component of the surface wind stress over the equatorial cold tongue in the observation is northward at all times (Hastenrath 1977; Wallace et al. 1989). The values shown in Fig. 5 are weaker than the annual mean from January through May and stronger in the remainder of the year. The

minimum value is in March and the maximum in September.

Figure 5 also shows that CTRL erroneously simulates a southward wind stress from January through May, as well as in December. This feature, which is associated with the double ITCZ syndrome that affects this CGCM as well as several others (Mechoso et al. 1995), only disappears entirely in the all-year experiment. The other two experiments still obtain a southward wind stress during a few months in the earlier part of the year. The curves in Fig. 5 differ primarily in their mean values. In reference to the annual variations, the weakest magnitudes are obtained in the all-year experiment.

In the remainder of this paper we examine surface wind rather than surface wind stress. The latter field is more meaningful for studies on atmosphere–ocean interactions. Nevertheless, we wish to compare our results with those provided by observational studies that emphasize the former field (e.g., Mitchell and Wallace 1992). The UCLA AGCM does not compute surface wind since the scheme of Deardorff (1972) calculates surface heat and momentum fluxes by using the PBL wind.

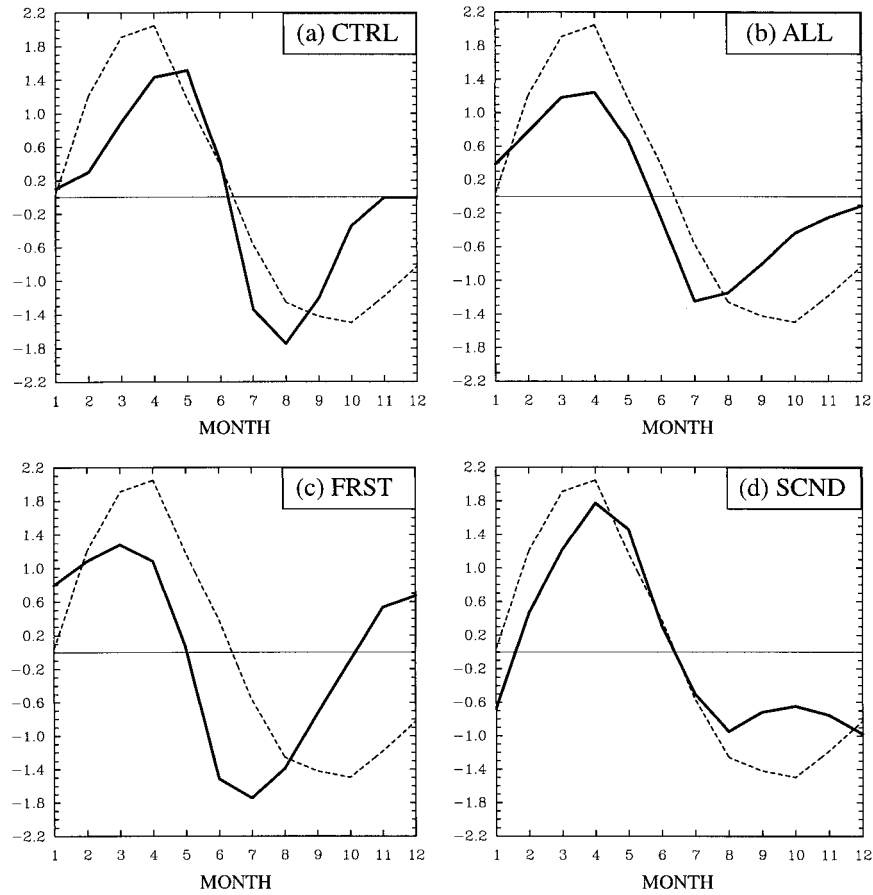


FIG. 4. Annual variations of SST averaged over the equatorial cold tongue obtained from (a) CTRL and the (b) all-year, (c) first-half-year, and (d) second-half-year experiments. The thin dashed curves in all panels are the annual variations from the observation.

Figure 6 shows the monthly mean PBL wind speed together with its zonal and meridional components over the equatorial cold tongue obtained in CTRL and in the second-half-year experiment. It is apparent that the annual variations of PBL wind speed in the second-half-year experiment are stronger than in CTRL. Concerning the zonal component, its annual variations are weak and erroneously dominated by the semiannual harmonic in CTRL, and they are stronger and more realistically dominated by the annual harmonic in the second-half-year experiment. Concerning the meridional wind component, its variations in the different experiments are consistent with those expected after inspection of Fig. 5. All of these features are relevant, as we will discuss later in this paper.

5. Impact on surface heat fluxes at the equator

Figure 7 displays the annual variations of surface heat flux into the ocean along the equator from the observation, from CTRL, and from the second-half-year experiment. In the far eastern sector (between 110° and 90° W) the observation shows that surface heat fluxes are larger than the annual mean from January through May and smaller in the remainder of the year (Fig. 7a). CTRL, on the other hand, produces heat fluxes that are larger than the annual mean from January through March and from July through December and smaller than the annual mean only from April through June (Fig. 7b). In terms of annual variations of heat flux into the ocean, therefore, CTRL underestimates values from Jan-

TABLE 1. Annual harmonic component in SST variations.

	Observation	Control simulation	All-year experiment	First-half-year experiment	Second-half-year experiment
Amplitude ($^{\circ}$ C)	1.76	1.15	1.08	1.38	1.23
Phase (degree)	282	297	308	341	268

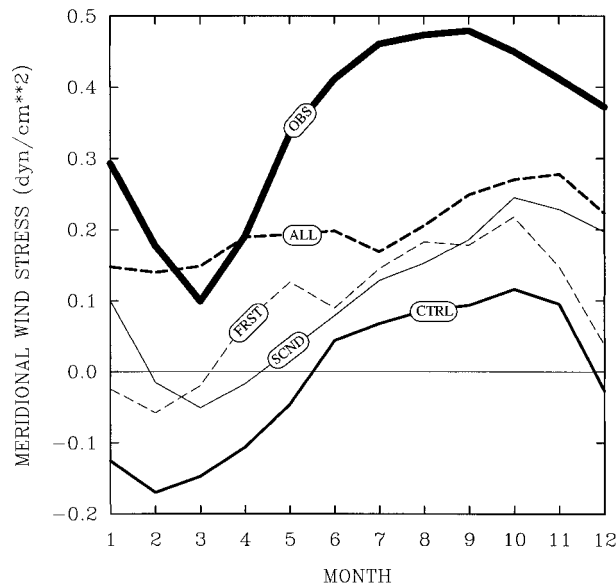


FIG. 5. Monthly mean meridional component of the surface wind stress over the equatorial cold tongue (between 120° and 90°W, and between S and N) from the FSU data (thick solid line), the control simulation (medium solid line), the all-year experiment (medium dashed line), the first-half-year experiment (thin dashed line), and the second-half-year experiment (thin solid line). Units are dyn².

uary through March and overestimates values from July through December. The errors are particularly large in the latter period, which corresponds to the cold phase of the equatorial cold tongue (see Fig. 3). Figure 7 also shows that the surface heat flux simulated by the second-half-year experiment in the eastern equatorial Pacific is more realistic than that produced by CTRL. In particular, this experiment captures the positive variations during the first months of the year during the warm phase of the equatorial cold tongue and the negative variations during the entire cold phase. The all-year experiment also produces an improvement of the annual variations in the latter period, but this is substantially smaller than that obtained in the second-half-year experiment (not shown). The first-half-year experiment produces results similar to CTRL (not shown). The different simulations of surface heat flux are consistent with the fact that only the second-half-year experiment can simulate the observed temporal asymmetries between the cold and warm phases of the equatorial cold tongue.

To gain more insight into these issues we examine the annual variations of the major components of the surface heat flux along the equator in the observation, in CTRL, and in the second-half-year experiment. Concerning the shortwave heat flux at the surface in the eastern Pacific (see Fig. 8), the observation shows a strong maximum in March and a minimum in July, with the negative values extending until the end of the year. A strong semiannual harmonic in the shortwave flux at the equator is expected from the local characteristics of

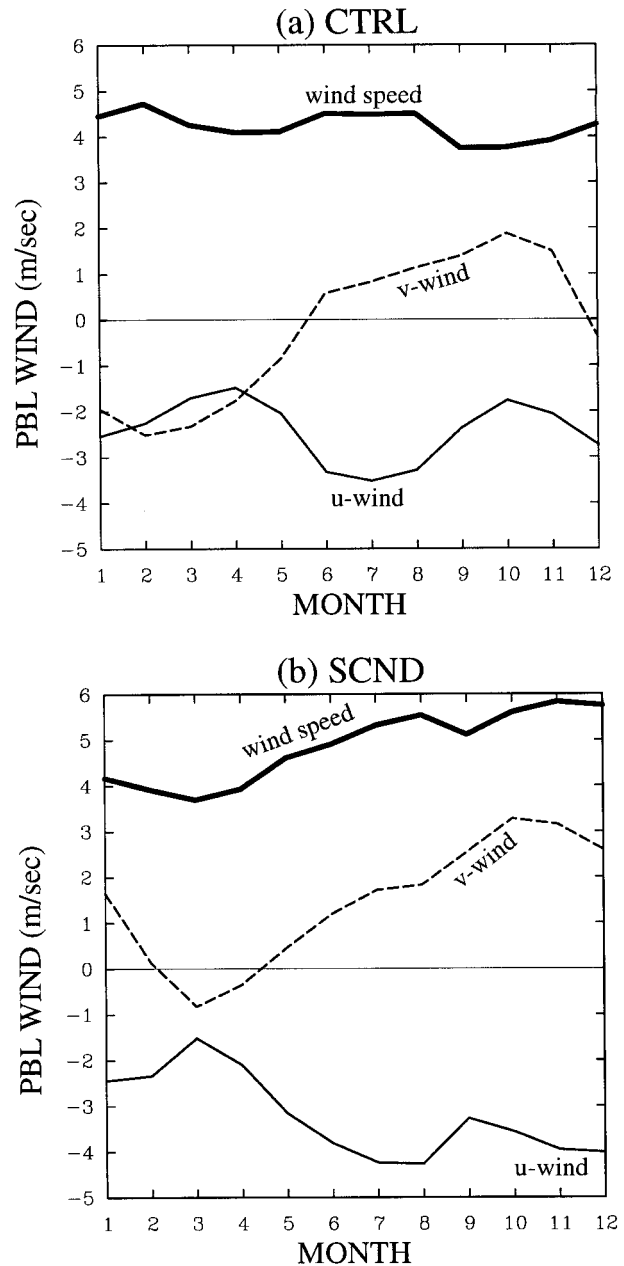


FIG. 6. Monthly mean PBL wind speed (thick solid lines) and of its zonal and meridional components (thin solid and thin dashed lines, respectively) over the cold tongue from (a) the control simulation and (b) the second-half-year experiment.

the seasonal cycle of insolation. Other harmonics appear due to variations in the Sun–Earth distance, as well as to changes in the characteristics of cloudiness. For example, the relative maximum of insolation east of 130°W around the September equinox is absent, probably due to enhanced low-level cloudiness. CTRL obtains a fairly similar behavior of shortwave heat flux at the surface except east of about 130°W, which emphasizes deficiencies in the simulation of low-level cloud-

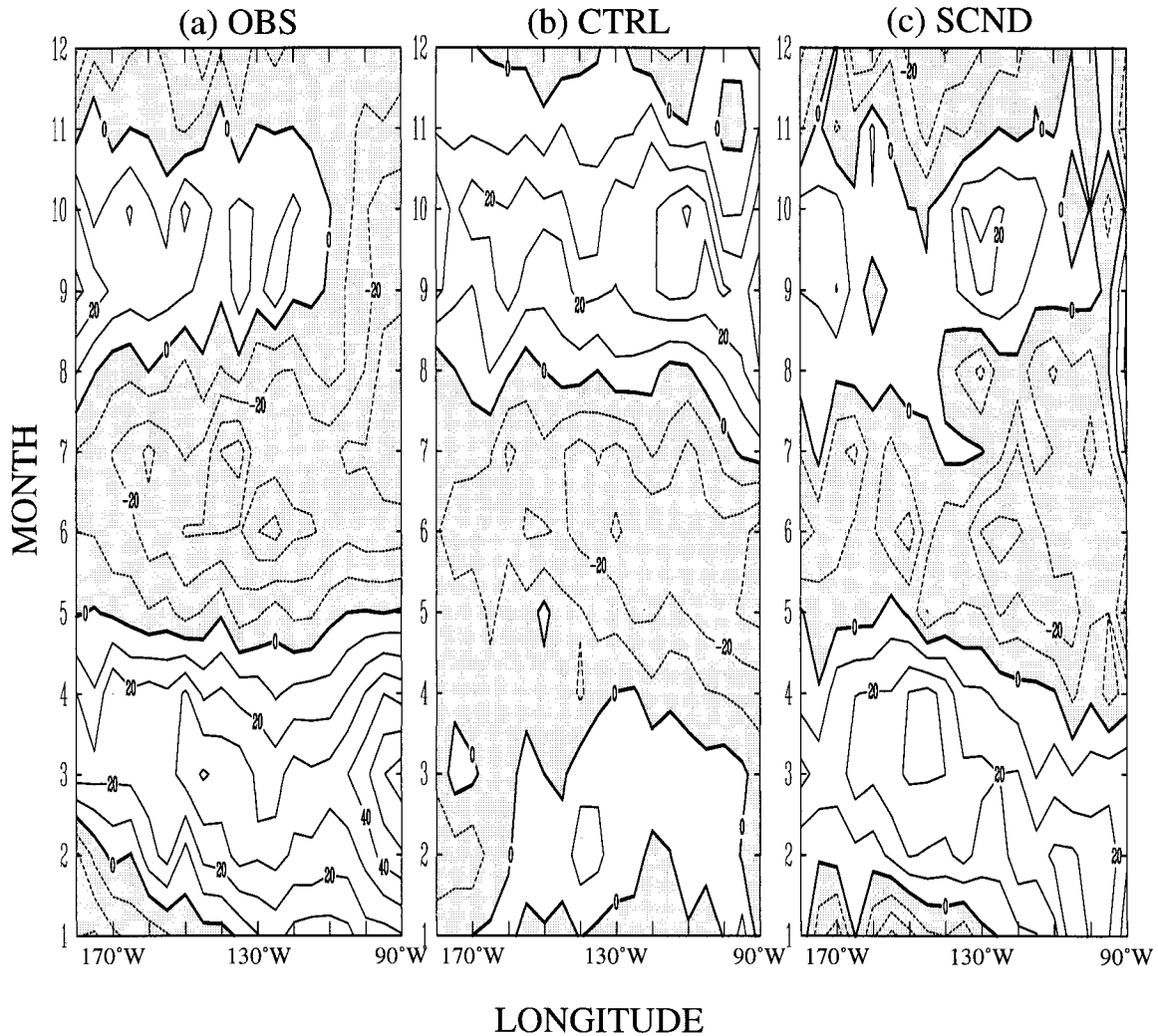


FIG. 7. Annual variations along the equator of monthly mean surface heat flux into the ocean from (a) the observation, (b) the control simulation, and (c) the second-half-year experiment. Values shown are averaged between 4°S and 4°N . Contour interval is 10 W m^{-2} . Negative values (surface heat flux out of the ocean) are shaded.

iness near the coast of South America. The shortwave flux produced in the second-half-year experiment, with the same treatment of cloudiness as in the AGCM, is practically identical to that obtained in CTRL. These results show that model errors in surface heat flux at the equator over the eastern sector receive an important contribution from those in its shortwave flux component.

Concerning the latent heat flux, we plot in Fig. 9 the annual variations of evaporation and SST over the equatorial cold tongue. The annual variations of evaporation in the observation and in CTRL are approximately out of phase. In the observation, except for May and June, evaporation is stronger (weaker) than the annual mean in months when SSTs are colder (warmer) than the annual mean. In observation, therefore, annual variations of evaporation over the equatorial cold tongue tend to

maintain or enhance those of SST. CTRL simulates a different relationship: evaporation is stronger (weaker) than the annual mean in months when SSTs are warmer (colder) than the annual mean. In the model, therefore, annual variations of latent heat flux tend to reduce or damp those of SST. Consistently, the cold phase ends too soon. The second-half-year experiment produces significantly more realistic annual variations of evaporation than CTRL, although the change in sign occurs too early and values are too weak after June. The enhanced surface evaporation in the second-half of the year is consistent with the longer-lasting cold phase of the cold tongue obtained in that experiment. In summary, the improvement in the duration of the cold phase of the equatorial cold tongue obtained in second-half-year experiment appears associated with a more realistic simulation of the surface latent heat flux.

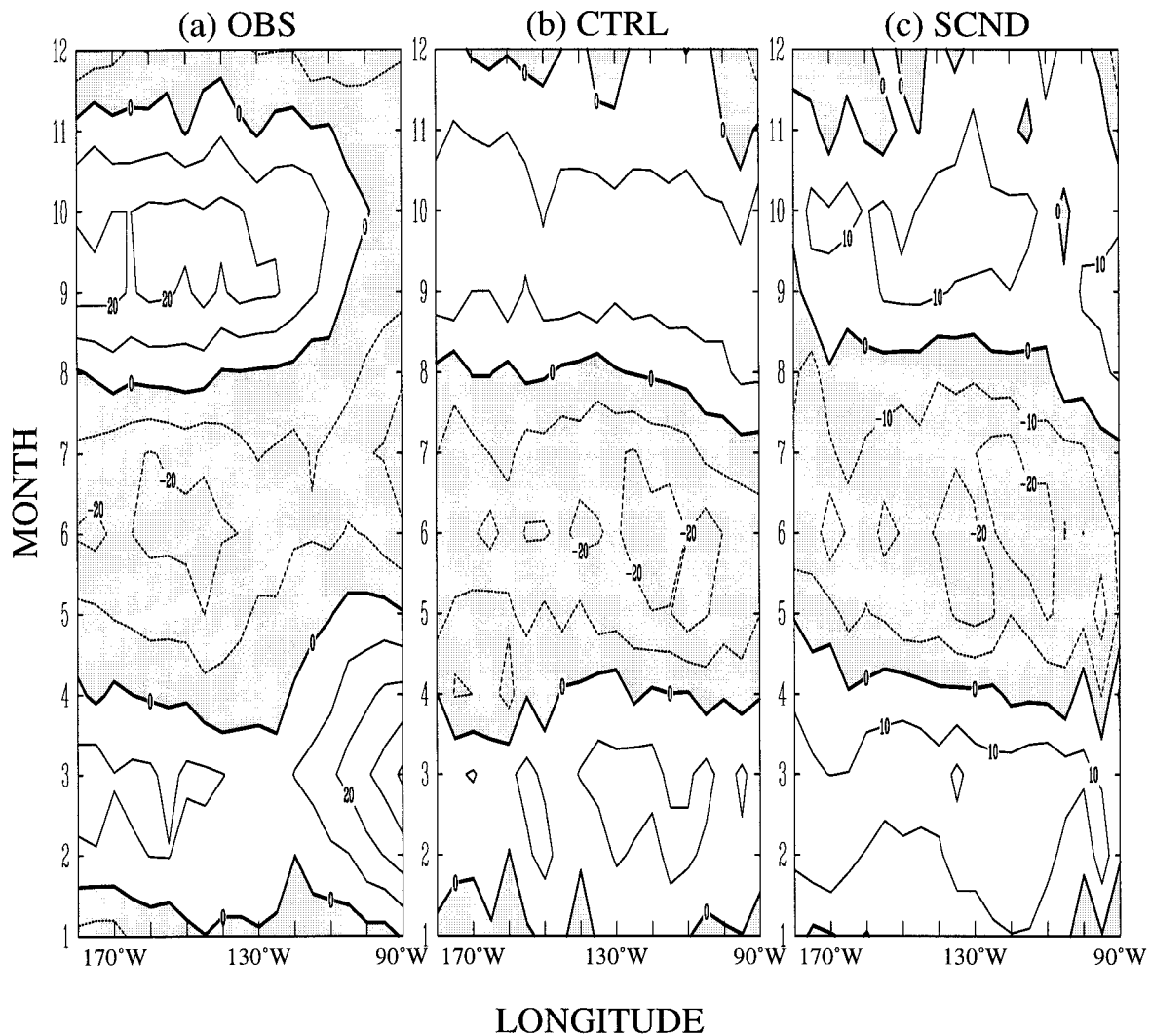


FIG. 8. As in Fig. 7, except for the shortwave radiative flux into the ocean. Contour interval is 10 W m^{-2} .

6. Discussion

We showed in section 3 that both the amplitude and temporal asymmetries of the annual variations of equatorial cold tongue SST are linked to the annual variations of Peruvian stratocumulus. We also showed in sections 4 and 5 that the annual variations of PBL wind and surface heat flux over the equatorial cold tongue are linked to those in Peruvian stratocumulus. Here we discuss the way in which those links are established. Consequently, the remainder of this section focuses on the results shown in Fig. 3.

To start with, we examine the poor model performance near the coast of South America, particularly in July and August. We recall that Mitchell and Wallace (1992) argue that the cold phase of the equatorial cold tongue appears in association with annual variations of the meridional component of the surface wind along the coast of South America. Southerly winds intensify at

the northward boundary of the cold tongue as the Central American monsoon develops in the second-half of the year. The local oceanic divergence at the equator is compensated by upwelling, which implies colder SSTs. Our results are consistent with this suggestion as the AGCM simulates strong convection and surface convergence over Central America in the Northern Hemisphere summer. The southeast–northwest tilt of the tropical Americas appears to be crucial in this respect.

In CTRL, the presence of too low SSTs in the far eastern Pacific during the cold phase of the equatorial cold tongue can be due to a combination of reasons involving deficiencies in the simulation of oceanic and atmospheric processes, as well as that of atmosphere–ocean feedbacks. It is well known that OGCMs have difficulties in successfully simulating the shallow mixed layer that characterizes the region. In CTRL, the divergence of the meridional component of the wind at

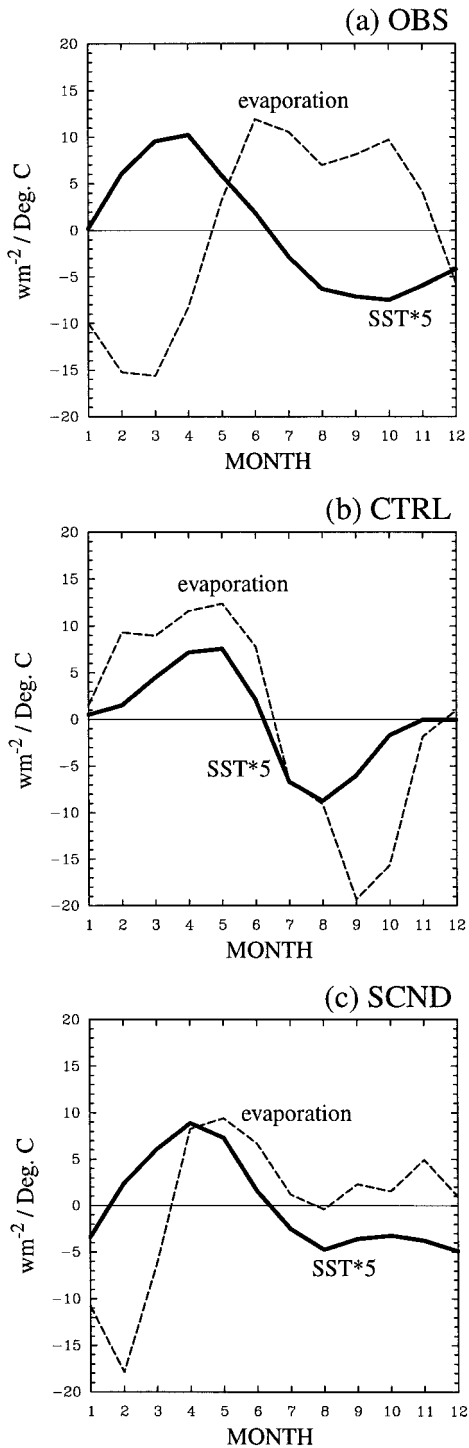


FIG. 9. Annual variations of monthly mean SST (solid lines) and evaporation (dashed lines) averaged over the cold tongue from (a) the observation, (b) the control simulation, and (c) the second-half-year experiment. Values of SST ($^{\circ}\text{C}$) are multiplied by 5. Units for evaporation are W m^2 .

the equator near the coast of South America is erroneously high as a spurious southern ITCZ develops and winds point away from the equator both to the north and to the south of it. The spurious divergence is decreased when stratus are enhanced and stronger southerly winds extend from the Peruvian coast up to the equator in all experiments. This effect is particularly intense around the middle of the calendar year when the double ITCZ is well developed (see Fig. 5 in Mechoso et al. 1995).

In support of these arguments we show in Fig. 10 the November–February mean sea level pressure and PBL winds produced by CTRL and the second-half-year experiment. It is apparent that southeastern trade winds strengthen south of the equator over the eastern Pacific when Peruvian stratocumulus are enhanced. This is associated with the intensification of a direct circulation over this part of the ocean by less absorption of insolation in the region of higher cloud incidence. Correspondingly, surface winds and lower-level advection of drier air intensify from the center of higher surface pressure under the stratocumulus clouds (Ma et al. 1996; Mechoso et al. 1998). Our results show the importance of the links between annual variations in the strength of this direct circulation and that of Peruvian stratocumulus coverage. This link between Peruvian and equatorial SST, therefore, is established through relationships between surface winds and upwelling or dynamical effects. The results obtained in the other two experiments are consistent with this scenario. The too cold SSTs are practically unchanged in the first-half-year experiment, in which flow changes occur at the wrong time of the year. The improvement is also detected in the all-year experiment, where similar processes are expected to develop.

Except for a narrow region adjacent to the coast of South America, CTRL produces an unrealistically early termination of the cold phase. As in Yu and Mechoso (1999) this simulation obtains an erroneous relationship between the annual variations of SST and surface latent heat flux over the equatorial cold tongue. Namely, the latter variations are primarily determined by those in near-surface wind speed in the observation, but in CTRL they are determined by the difference between the mean specific humidity in the PBL and the saturated specific humidity corresponding to the underlying SST (Fig. 9). The model produces an almost constant PBL wind speed albeit the zonal and meridional PBL wind components are far from constant (see Fig. 6a). The presence of Peruvian stratocumulus in the second-half of the year results in more realistic zonal and meridional components of the PBL winds over the equatorial cold tongue, particularly during the last and the earlier months of the calendar year. The annual variations in PBL wind speed are stronger and more realistic. Therefore, the monthly variations of the latent heat flux over the cold tongue follow more closely those in wind speed than those in the humidity difference (see Fig. 11). This improvement

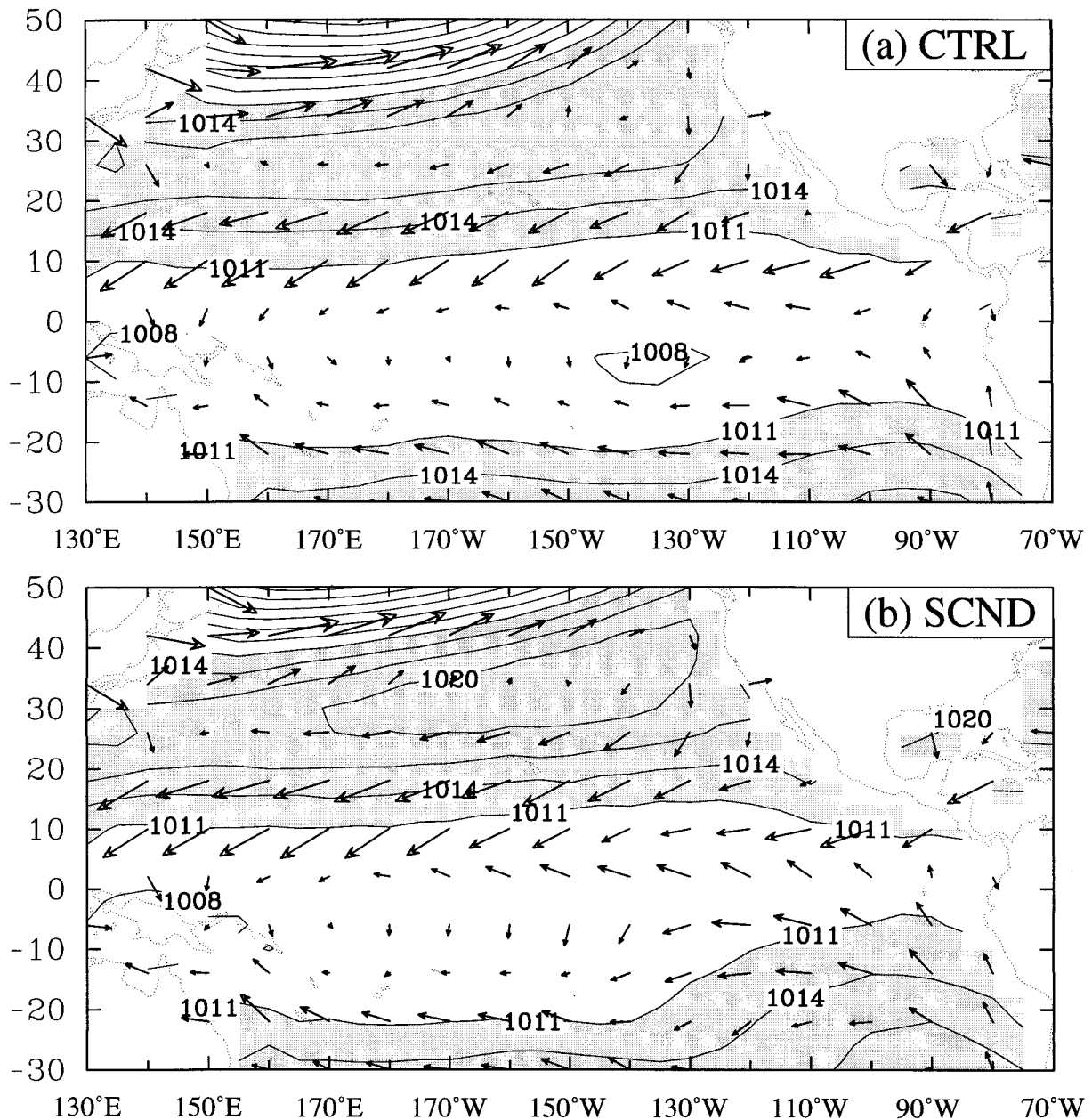


FIG. 10. Nov–Feb mean sea level pressure (contours) and PBL wind speed (arrows) from (a) the control simulation and (b) the second-half-year experiment. Contour intervals are 3 mb. Values larger than 1011 mb are shaded.

changes the relationship between SST and surface evaporation from a negative feedback in CTRL to a positive feedback in the second-half-year experiment. A longer-lasting cold phase of the cold tongue is thus obtained, and the observed temporal asymmetry in the annual variations of the eastern equatorial Pacific SSTs is produced. This link between Peruvian stratocumulus and equatorial SST, therefore, is established through surface evaporation or thermal effects. Again, the results obtained in the other two experiments are consistent with this scenario.

The simple coupled model study of Li and Philander (1996) suggested that the marked asymmetry, relative to the equator, of the annual mean climate is the principal reason for the pronounced annual cycle of SST in the eastern equatorial Pacific. They further suggested that the amplitude of the annual cycle depends on air–sea interactions, such as wind-enhanced surface evaporation, wind-induced upwelling, and the positive feedback between SST and low-level cloudiness. The current study finds that the all-year experiment produces the strongest asymmetry relative to the equator in the annual mean

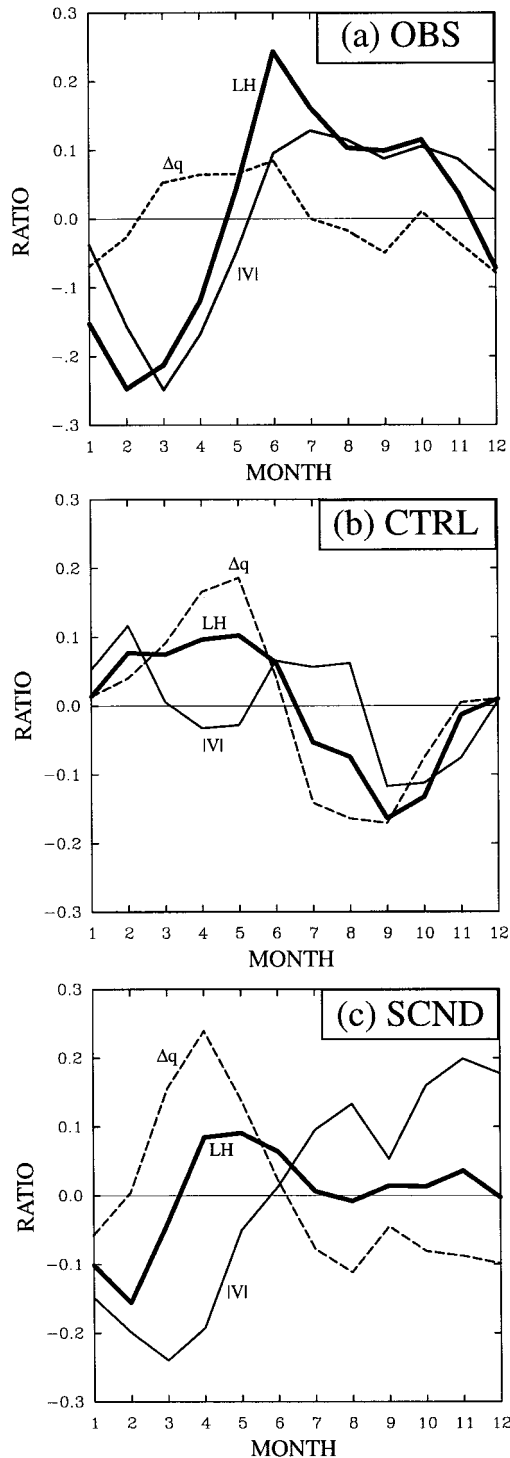


FIG. 11. Annual variations of monthly mean evaporation (thick solid lines; labeled "LH"), wind speed near the surface or in the PBL (thin lines; labeled " $|V|$ "), and difference between specific humidity in the PBL and that corresponding to the underlying SST (thin dashed lines; labeled " Δq ") over the cold tongue from (a) the observation, (b) the control simulation, and (c) the second-half-year experiment. Values are expressed as a percentage of the corresponding annual means.

SST distribution in the eastern Pacific (see Figs. 1 and 2) but the weakest annual harmonics in the equatorial cold tongue SST. Therefore, there is a need to look into the relative importance of air–sea interaction processes in determining the amplitude of the annual cycle.

Concerning the importance of the wind-enhanced surface evaporation process, in section 5 it was shown that all model simulations except the second-half-year experiment produce unrealistic annual variations of surface evaporation over the equatorial cold tongue. The annual variations in evaporation produced in CTRL are opposite from those in the observations. However, CTRL and the second-half-year experiment have similar annual cycle amplitudes in SST (see Table 1). Therefore, surface evaporation does not appear to be the dominant process that determines the amplitude of the annual cycle. This is consistent with the finding of Nigam and Chao (1996), who argued that surface evaporation plays a secondary role in the annual march of SST in the eastern equatorial Pacific. Our study finds the wind-enhanced evaporation process is primarily responsible for generating the temporal asymmetries between the warm and cold phases in the annual cycle. Concerning the importance of the wind-induced upwelling process, in section 4 it was shown that all model simulations except the all-year experiment produce similar amplitudes in the annual variations of meridional wind stress over the equatorial cold tongue. This similarity suggests that CTRL and the first-half-year and the second-half-year experiments may have similar annual variations in upwelling over the equatorial cold tongue. This is consistent with the similar annual cycle amplitudes of SST produced in those simulations (see Table 1). Apparently, the weak annual cycle amplitude produced in the all-year experiment is linked to its weak annual variations of meridional wind stress. Since all model simulations significantly underestimate low-level clouds over the equatorial cold tongue, the low-level cloud feedback processes cannot be responsible for the differences seen among the model simulations. In summary, the current study suggests that the wind-induced upwelling process (i.e., the dynamical effect) may be the most important air–sea interaction process that affects the amplitude of the annual cycle in the eastern equatorial Pacific.

The situation in nature is somewhere between the idealizations made in the all-year and second-half-year experiments. There are Peruvian stratocumulus at all times of the year, but their incidence is higher in the second half of the year. Consistently, the annual mean SSTs are more realistic in the all-year experiment and the annual variations of SST are more realistic in the second-half-year experiment.

7. Conclusions

This study examined the hypothesis that Peruvian stratocumulus play an important role on both the annual mean and annual variations of SST in the eastern equa-

torial Pacific. We addressed this problem by performing sensitivity experiments with the UCLA coupled atmosphere–ocean GCM.

In further agreement with Ma et al. (1996), our results are consistent with the notion that Peruvian stratocumulus are a key component of the interhemispherically asymmetric features of the eastern equatorial Pacific climate. In the context of a model CGCM whose AGCM component generally underestimates stratocumulus coverage and incidence even with prescribed SSTs, only if stratus are prescribed off the Peruvian coast do simulated SSTs cool down to values comparable to those in the observation and is the double ITCZ syndrome alleviated. Our principal new finding is that the annual variations of Peruvian stratocumulus are linked to the temporal asymmetries between the warm and cold phases of the equatorial cold tongue. Again in the model's context, only if the prescribed annual variations are in phase with the observation are the amplitude, duration, and westward propagation speed of the warm and cold phases of the equatorial cold tongue similar to those in the observation.

The impact of Peruvian stratocumulus on equatorial SST involves dynamical and thermal effects. The dynamical effects develop through the relationships between southerly surface winds over the equatorial cold tongue and higher surface pressures over the cool waters underneath the stratocumulus decks along the coast of South America. The thermal effects develop through the special relationships between surface evaporation and surface wind speed over the equatorial cold tongue, which contributes to extend the cold phase until the end of the year. The behavior of those winds is linked to that of Peruvian stratocumulus.

The results of this study emphasize the need for improved simulations of cloudiness with CGCMs. In particular, these models must capture the seasonal cycle of Peruvian stratocumulus in order to produce realistic simulations of the annual variations of SSTs and to capture the atmosphere–ocean feedback in the eastern equatorial Pacific. Qualitatively similar conclusions are expected to apply in the eastern equatorial Atlantic, where stratocumulus are also a pervasive feature of the regional climate.

Acknowledgments. The authors would like to thank Professor A. Arakawa for his interest during this study and Professor G. S. Philander for several stimulating discussions. Comments from Dr. Steve Klein and an anonymous reviewer also helped improve the manuscript. Dr. C.-C. Ma helped to set up the CGCM experiments. Support was provided by NOAA GOALS Grant NA66GP0121 and by the Campus Laboratory Cooperation project of DOE and the University of California. Model integrations were performed at the San Diego Supercomputer Center and the Climate Simulation Laboratory at NCAR.

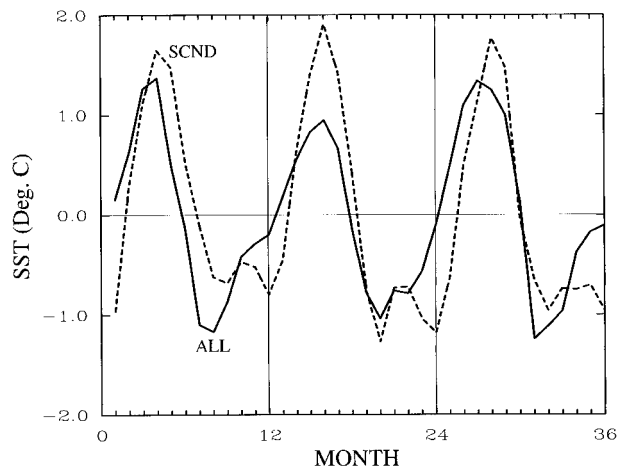


FIG. A1. Temporal evolutions of the monthly mean SSTs produced by the all-year (solid) and second-half-year (dashed) experiments over the equatorial cold tongue.

APPENDIX

Interannual Variability

The length of model integration selected for analysis (3 yr) may be too short in view of the potential of the coupled atmosphere–ocean system for producing variability on comparable timescales. Figure A1 shows that this potential is not realized. The figure confirms the longer duration of the cold phase of the equatorial cold tongue in the second-half-year experiment. The weakest amplitudes are obtained in the all-year experiment, as expected.

REFERENCES

- Alexander, R. C., and R. L. Mobley, 1976: Monthly average sea-surface temperatures and ice-pack limits on a 1° global grid. *Mon. Wea. Rev.*, **104**, 143–148.
- Arakawa, A., and W. H. Schubert, 1974: Interaction of a cumulus cloud ensemble with the large-scale environment, Part I. *J. Atmos. Sci.*, **31**, 674–701.
- Battisti, D. S., and A. C. Hirst, 1989: Interannual variability in a tropical atmosphere–ocean model: Influence of the basic state, ocean geometry and nonlinearity. *J. Atmos. Sci.*, **46**, 1687–1712.
- Bryan, K., 1969: A numerical method for the study of the circulation of the world ocean. *J. Comput. Phys.*, **4**, 347–376.
- Cox, M. D., 1984: A primitive equation three-dimensional model of the ocean. GFDL Ocean Group Tech. Rep. 1. [Available from Geophysical Fluid Dynamics Laboratory, P. O. Box 308, Princeton, NJ 08542-0308.]
- Deardorff, J. W., 1972: Parameterization of the planetary boundary layer for use in general circulation models. *Mon. Wea. Rev.*, **100**, 93–106.
- Harshvardhan, R. D., D. A. Randall, and T. G. Corsetti, 1987: A fast radiation parameterization for general circulation models. *J. Geophys. Res.*, **92**, 1009–1016.
- Hastenrath, S., 1977: On the upper air circulation over the equatorial Americas. *Arch. Meteor. Geophys. Bioklimatol.*, **25A**, 309–321.
- Jin, F.-F., J. D. Neelin, and M. Ghil, 1994: El Niño on the devil's staircase: Annual subharmonic steps to chaos. *Science*, **264**, 70–72.
- Katayama, A., 1972: A simplified scheme for computing radiative

- transfer in the troposphere. Numerical Simulation of Weather and Climate Tech. Rep. 6, Dept. of Atmospheric Sciences, University of California, Los Angeles, 77 pp. [Available from Dept. of Atmospheric Sciences, University of California, Los Angeles, Los Angeles, CA 90024.]
- Kim, Y.-J., and A. Arakawa, 1995: Improvement of orographic gravity wave parameterization using a mesoscale gravity wave model. *J. Atmos. Sci.*, **52**, 1875–1902.
- Klein, S. A., and D. L. Hartmann, 1993: The seasonal cycle of low stratiform clouds. *J. Climate*, **6**, 1587–1606.
- Legler, D. M., and J. J. O'Brien, 1984: *Atlas of Tropical Pacific Wind Stress Climatology 1971–1980*. Dept. of Meteorology, The Florida State University, 182 pp.
- Li, T., and S. G. H. Philander, 1996: On the annual cycle of the eastern equatorial Pacific. *J. Climate*, **9**, 2986–2998.
- Ma, C.-C., C. R. Mechoso, A. W. Robertson, and A. Arakawa, 1996: Peruvian stratus clouds and the tropical Pacific circulation: A coupled ocean–atmosphere GCM study. *J. Climate*, **9**, 1635–1645.
- Mechoso, C. R., and Coauthors, 1995: The seasonal cycle over the tropical Pacific in general circulation models. *Mon. Wea. Rev.*, **123**, 2825–2838.
- , J.-Y. Yu, and A. Arakawa, 1998: A coupled GCM pilgrimage: From climate catastrophe to ENSO simulations. *General Circulation Model Development: Past, Present, and Future: Proceedings of a Symposium in Honor of Professor Arakawa*, D. A. Randall, Ed., Academic Press, in press.
- Mellor, G. L., and T. Yamada, 1982: Development of a turbulence closure model for geophysical fluid problems. *Rev. Geophys. Space Phys.*, **20**, 851–875.
- Mitchell, T. P., and J. M. Wallace, 1992: On the annual cycle in equatorial convection and sea surface temperature. *J. Climate*, **5**, 1140–1156.
- Neelin, J. D., 1991: The slow sea surface temperature mode and the fast-wave limit: Analytic theory for tropical interannual oscillations and experiments in a hybrid coupled model. *J. Atmos. Sci.*, **48**, 584–606.
- Nigam, S., and Y. Chao, 1996: Evolution dynamics of tropical ocean–atmosphere annual cycle variability. *J. Climate*, **9**, 3187–3205.
- Oberhuber, J. M., 1988: An atlas based on the COADS data set: The budgets of heat buoyancy and turbulent kinetic energy at the surface of the global ocean. Max-Planck Institut für Meteorologie Rep. 15. [Available from Max-Planck Institut für Meteorologie, Bundesstrasse 55, 2000 Hamburg 13, Germany.]
- Pacanowski, R. C., K. W. Dixon, and A. Rosati, 1991: The GFDL Modular Ocean Model user guide. GFDL Ocean Group Tech. Rep. 2. [Available from Geophysical Fluid Dynamics Laboratory, P. O. Box 308, Princeton, NJ 08542-0308.]
- Philander, S. G. H., D. Gu, D. Halpern, G. Lambert, N.-C. Lau, T. Li, and R. C. Pacanowski, 1996: Why the ITCZ is mostly north of the equator. *J. Climate*, **9**, 2958–2972.
- Robertson, A. W., C.-C. Ma, C. R. Mechoso, and M. Ghil, 1995: Simulation of the tropical Pacific climate with a coupled ocean–atmosphere general circulation model. Part I: The seasonal cycle. *J. Climate*, **8**, 1178–1198.
- Suarez, M. J., A. Arakawa, and D. A. Randall, 1983: The parameterization of the planetary boundary layer in the UCLA general circulation model: Formulation and results. *Mon. Wea. Rev.*, **111**, 2224–2243.
- Tziperman, E., L. Stone, H. Jarsoh, and M. A. Cane, 1994: El Niño chaos: Overlapping of resonances between the seasonal cycle and Pacific ocean–atmosphere oscillator. *Science*, **264**, 72–74.
- Wallace, J. M., T. P. Mitchell, and C. Deser, 1989: The influence of sea-surface temperature on surface wind in the eastern equatorial Pacific: Seasonal and interannual variability. *J. Climate*, **2**, 1492–1499.
- Woodruff, S. D., R. J. Slutz, R. J. Jenne, and P. M. Stenrer, 1987: A Comprehensive Ocean–Atmosphere Data Set. *Bull. Amer. Meteor. Soc.*, **68**, 1239–1250.
- Yu, J.-Y., and C. R. Mechoso, 1999: A discussion on the errors in the surface heat fluxes simulated by a coupled GCM. *J. Climate*, **12**, 416–426.